Low Reynolds number effects on aerodynamic loads of a small scale wind turbine

Hakjin Lee[a] and Duck-Joo Lee[b,*]

[a] Mechanical Engineering Research Institute, Korea Advanced Institute of Science and Technology (KAIST), Daejeon, 34141, Republic of Korea

[b] Department of Aerospace Engineering, Korea Advanced Institute of Science and Technology (KAIST), Daejeon, 34141, Republic of Korea

Abstract

Small-scale or scaled-down wind turbines for model experiments mostly operate in low-Reynolds-number flow. The nonlinear variations of aerodynamic coefficients with respect to the angle of attack caused by viscous effects and laminar boundary layer separation affect the wind turbine performance under these conditions. Although the vortex lattice method (VLM) is an efficient way to predict rotor performance, it tends to suffer from numerical error because nonlinear aerodynamic characteristics cannot be considered. In this study, the nonlinear vortex lattice method (NVLM) is adopted to compute the aerodynamic loads of two small-scale wind turbines. This method involves a sectional airfoil look-up table and vortex strength correction and can be applied to a wide range of operating conditions. The simulations of TU Delft and NTNU wind turbines are conducted to validate the prediction capability of numerical models by comparing predictions with the measurements. It was found that the overall results from the NVLM simulation are more accurate than the VLM results, which implies that the nonlinear aerodynamic characteristics associated with low-Reynolds-number flow should be considered to accurately assess the aerodynamic performance of small-sized wind-turbines, particularly at the low tip speed ratio at which the rotor blade may experience flow separation and dynamic stall.

Keywords: Small scale wind turbine; Low Reynolds number flow; Nonlinear aerodynamic characteristics; Wind turbine aerodynamics; Nonlinear vortex lattice method; Vortex particle method.

[*] Corresponding author. KAIST, 291 Daehak-ro, Yuseng-gu, Daejeon 34141, Republic of Korea.
E-mail: djlee@kaist.ac.kr (Duck-Joo Lee)

1. Introduction

Measurements of wind turbines have provided insightful information needed to understand the fundamental flow physics occurring around them. In addition, measured data help to enhance the predictive capability of numerical models for wind turbines. Many experimental studies have been conducted to estimate overall wind turbine performance and investigate the underlying flow behavior around the rotor blades. At first, measurements of wind turbines had been taken under uncontrolled wind conditions in which the level of turbulence, direction, and magnitude of wind speed continuously and randomly changed with respect to time. The recorded results in the natural environment suffered from considerable uncertainty. Hence, the experimental data acquired from a field test were not able to be directly compared with the predicted results by numerical simulation. To resolve the aforementioned problems related to the stochastic nature of the atmosphere, experimental studies have been carried out in wind tunnel facilities where wind conditions can be well-controlled. One of the advantages of measurements taken under controlled conditions is that the experiments can produce a high-quality database regarding rotor aerodynamics, wake development, and wind turbine noise. The NREL Phase VI experiment with a 10-m-diameter two-bladed model was conducted in a 24.4 m × 36.6 m NASA-Ames wind tunnel facility in 2000 [1]. The main purpose of this test was to acquire extensive aerodynamic measurements on a wind turbine model for a wide range of wind speeds involving fully attached and separated flow conditions. In addition, the NREL wind turbine model operated under yawed inflow conditions, resulting in highly unsteady aerodynamic loads on the rotor blades. NREL measurements have provided a comprehensive aerodynamic database including integrated turbine performance, surface pressure, normal, and tangential forces acting on the wind turbine blades. Extensive measurements on MEXICO (model rotor experiments in controlled conditions) a 4.5-m-diameter wind turbine with a three-bladed model has been conducted in the 9.5 m × 9.5 m open section of the Large Low-Speed Facility (LLF) of the German-Dutch Wind Tunnels (DNW) in 2006 [2] and 2014 [3]. Compared with the NREL Phase VI wind tunnel test, this campaign offered a database of detailed aerodynamic measurements on the three-bladed wind turbine. In addition, the main feature of the MEXICO experiments is that the measurements on three-dimensional flow fields in terms of velocity components around the rotor blades and the trajectories of the tip vortices were taken using the stereo particle image velocimetry (PIV) technique and PIV vortex tracking, respectively. The comprehensive database acquired from two wind tunnel tests under controlled wind conditions were used as a data set for blind code comparison or model validation, such as blade element momentum (BEM)

theory [4, 5], actuator disk or actuator line theories [6–8], vortex methods [9–14], and computational fluid dynamics (CFD) methods [15–21]. Experiments on the 1.2-m-diameter scaled-down wind turbine with a two-bladed model have been performed in an open jet tunnel at Delft University of Technology (DUT) [22–25]. The primary objective of this measurement was to investigate the aerodynamic performance and near-wake dynamics of a small-scale wind turbine under axial- and yawed-flow conditions. Thrust forces normal to the rotating plane were recorded by the strain gauges, and the effects of tip speed ratio, tip pitch angle, and yaw angle on the thrust force were discussed in detail. During the experiment, the trajectories of the tip vortices were identified by the flow visualization technique. This information facilitated a deeper investigation into the near-wake behavior of the horizontal-axis wind turbine, particularly at the impacts of skewed wake geometries induced by the yawed inflow. Another set of small-scale wind turbine experiments has been conducted in the large-scale closed-loop wind tunnel facility of the Norwegian University of Science and Technology (NTNU) by joint Norwegian research programs on wind turbine technology, denoted Nowitech and Norcowe, in 2011 [26] and 2012 [27]. A three-bladed wind turbine model with a diameter of 0.894 m was used. This experiment provided reliable and useful flow field data, including the normalized mean velocity defect and turbulent kinetic energy at the downstream region as well as integrated turbine performance.

The major feature of the TU Delft and NTNU experiments is that the wind turbine models operate at a low Reynolds number based on chord length, as the blade diameter is relatively small. For a range of low Reynolds numbers, flow over the rotor blade is much more sensitive to external disturbances, and viscous effects are a dominant factor in determining the flow characteristics around the airfoil involved in the blade section of wind turbines. A strong adverse pressure gradient along the streamwise direction, caused by viscous effects, makes the laminar boundary layer separate from the upper surface of the airfoil. In addition, external disturbances in the boundary layer cause the separated laminar flow to transition into the turbulent state. Turbulent flow tends to reattach on the surface of the airfoil, accompanying the laminar separation bubbles (LSB), where the separated laminar flow and turbulent flow simultaneously exist in the form of circulating flow within the closed volume. Consequently, LSB characterized by a slow recirculating flow directly affect the aerodynamic performance of the airfoil, generally in a negative manner, through the appearance of pressure fluctuations and drag penalties. Furthermore, when the airfoil encounters the low-Reynolds-number flow, nonlinear behavior of aerodynamic coefficients with respect to the angle of attack occurs, as shown in Fig. 1, where the lift and drag coefficients at both high and low Reynolds numbers were obtained from the numerical simulations using XFOIL. Fig. 1 show that the variations of aerodynamic coefficients are significantly different depending on the Reynolds number.

Hence, these nonlinear aerodynamic characteristics associated with the low-Reynolds-number flow should be considered to accurately predict the rotor performance of a model wind turbine.

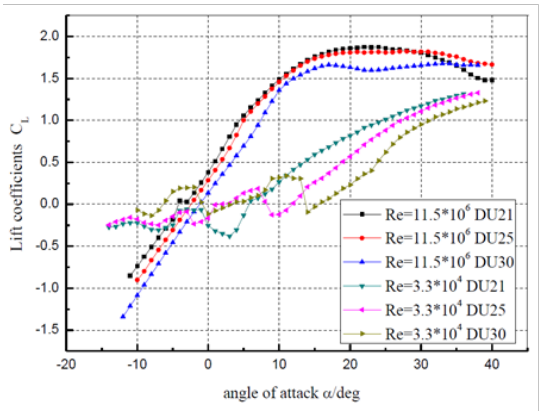

(a) Lift coefficients of the airfoil

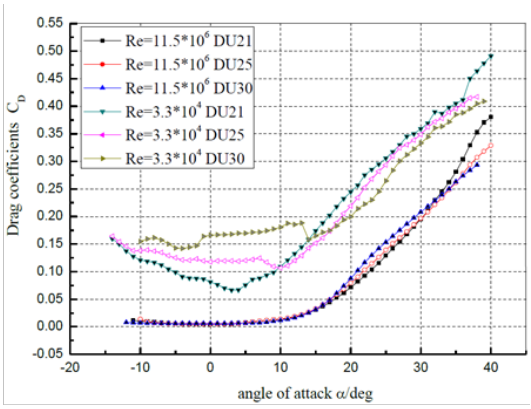

(b) Drag coefficients of the airfoil

Fig. 1. Effect of Reynolds number on lift and drag coefficients of the airfoil [28] (retrieved from Du et al.)

Predicting aerodynamic loads generated from the wind turbine blade using numerical models is important for validating and verifying the measured data. In addition, this information can help to improve our understanding of the complicated flow physics occurring around the rotor blades of wind turbines. The main aim of this study is to numerically predict the aerodynamic performance of two small wind turbines, particularly one operating under low-Reynolds-number flow. In this study, the nonlinear vortex lattice method (NVLM) coupled with a time-accurate vortex particle method (VPM) is used because the conventional vortex lattice method (VLM) cannot handle the nonlinear variation in lift coefficients caused by the low-Reynolds-number effects. Hence, VLM is insufficient to apply for the scaled-down model simulation, even though VLM is one of the most preferable methods for aerodynamic analysis of full-scale turbines or helicopters, which mostly operate under relatively

high-Reynolds-number flow. NVLM has been suggested for analyzing the aerodynamics and wake dynamics of the horizontal-axis wind turbine with high accuracy and affordable computing cost. It is capable of handling nonlinear aerodynamic characteristics, which are mainly associated with viscous effects, stalled flow, and low-Reynolds-number flow, by incorporating a sectional airfoil look-up table and vortex strength correction [13, 14, 29]. Two small-scale wind-turbines, TU Delft and NTNU, are considered to reveal how low-Reynolds-number flow affects aerodynamic loads. Calculations for two wind-turbine configurations are compared against the measurements, and they are used to validate the predictive capability of the numerical models. It is found that serious discrepancies are observed in the VLM simulations, whereas NVLM yields more accurate results, including nonlinear aerodynamic loads and wake structures.

2. Numerical methods and modeling

2.1 Nonlinear vortex lattice method

Vortex methods would be a better approach to analyzing the wind turbine aerodynamics and wake dynamics, as the rotor blades of the wind turbine mostly operate in incompressible flow. Generally, they can provide more reliable solutions than blade element momentum (BEM) theory and more cost-effective solutions than CFD methods. In addition, vortex methods have a great ability to model the wake structures without numerical dissipation error. Among the various models, VLM is one of the most practical approaches to the comprehensive analysis of rotary systems, such as those of the helicopter blade, propeller, and wind turbine blade. VLM is based on the assumption of thin lifting surface theory. If the rotor blade is assumed to be thin, then it can be regarded as a lifting surface without a thickness. The rotor blades are modeled using the chordwise and spanwise distributions of quadrilateral vortex ring elements, consisting of four concentrated (lumped) vortex filaments, as depicted in Fig. 2. A vortex ring element with the strength of the circulation ($\Gamma_{i,j}$) is assigned, corresponding to each panel, where i and j imply the indices in the chordwise and spanwise directions, respectively. The unknown strength of bound circulation on the rotor blades at each time step is calculated by enforcing the zero normal flow condition at the collocation point of each vortex element as in Eq. (1). Here, ϕ is the velocity potential and $\mathbf{V}$ is the time-dependent kinematic velocity, which is the sum of the freestream velocity ($\mathbf{V}_\infty$) and blade rotational velocity ($\mathbf{\Omega} \times \mathbf{r}$) at each collocation point, $\mathbf{n}$ is the unit normal vector of each vortex ring elements, and $\mathbf{V}_{\text{ind.blade}}$ and $\mathbf{V}_{\text{ind.wake}}$ indicate the velocity components induced by bound vortices on the rotor blades and wake vortices, respectively. Consequently, the time-dependent boundary condition for unsteady rotor simulation is as expressed in Eq. (2).

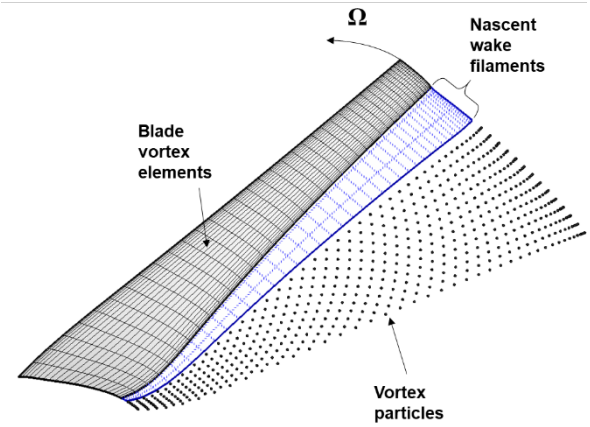

Fig. 2. Vortex elements for a wind turbine rotor blade

$$(\nabla\phi + \mathbf{V})\cdot\mathbf{n} = 0 \qquad \text{Eq. (1)}$$

$$(\mathbf{V}_{\text{ind.bound}} + \mathbf{V}_{\text{ind.wake}} + \mathbf{V}_{\infty} - \boldsymbol{\Omega}\times\mathbf{r})\cdot\mathbf{n} = 0 \qquad \text{Eq. (2)}$$

If the boundary condition is specified on the collocation points of each vortex element, a linear system of equations for the strength of bound vortices can be established, as shown in Eq. (3)–(5). The unknown strength of circulation distributed on the rotor blade is determined by solving a linear system of equations, satisfying the instantaneous boundary condition at each time step. Once the bound vorticity on the rotor blade is determined, the resulting aerodynamic loads generated by the rotor blade can be calculated by using the unsteady Kutta–Joukowski theorem [30].

$$\begin{pmatrix} a_{11} & a_{12} & \cdots & a_{1m} \\ a_{21} & a_{22} & \cdots & a_{2m} \\ \vdots & \vdots & \ddots & \vdots \\ a_{m1} & a_{m2} & \cdots & a_{mm} \end{pmatrix} \begin{pmatrix} \Gamma_1 \\ \Gamma_2 \\ \vdots \\ \Gamma_m \end{pmatrix} = \begin{pmatrix} \text{RHS}_1 \\ \text{RHS}_2 \\ \vdots \\ \text{RHS}_m \end{pmatrix} \qquad \text{Eq. (3)}$$

$$RHS_i = -(\mathbf{V}_{\text{ind.wake}} + \mathbf{V}_{\infty} - \boldsymbol{\Omega}\times\mathbf{r})_i \cdot \mathbf{n}_i \qquad \text{Eq. (4)}$$

$$a_{ij} = (\mathbf{V}_{\text{ind.bound}})_{ij} \cdot \mathbf{n}_i \qquad \text{Eq. (5)}$$

Here, a_{ij} corresponds to the combination of influence coefficients, defined as the velocity component normal to the surface induced by the *j*-th vortex ring element with unit strength to the collocation point of the *i*-th vortex ring element. *m* is the number of total vortex ring elements and is defined as $m = MN$ where *M* and *N* are the number of vortex ring elements in the chordwise and spanwise directions, respectively.

VLM is an efficient way to compute the aerodynamic loads acting on the rotor blade and describe the wake behavior of wind turbines. However, the nonlinear aerodynamic characteristics caused by low-Reynolds-number flow and viscous effects cannot be intrinsically considered because VLM is based on the potential flow. Hence, VLM tends to suffer from numerical errors that appear when the small-scale wind turbine operates at low-Reynolds-number flow. To overcome the inherent drawbacks of VLM mentioned above, NVLM is adopted to predict the aerodynamic performance of the small-size wind-turbine models. This can be possible by incorporating an airfoil look-up table, which is a practical and efficient way to consider the aerodynamic behavior of airfoils. To determine sectional aerodynamic coefficients, sectional flow conditions including the local inflow velocity ($\mathbf{V}_{\text{inflow}}$) and effective angle of attack (α_{eff}), as in Eq. (6) and Eq. (7), are evaluated from VLM potential solutions. Here α_{inflow} is the inflow angle and θ_{geo} is the geometric angle of attack at the control points, which is composed of the local twist angle (θ_{twist}) and blade pitch angle (θ_{pitch}). $\mathbf{a_1}$ and $\mathbf{a_3}$ are the unit vectors tangential and normal to the rotating plane, respectively. The sectional lift (C_L) and drag (C_D) coefficients can be obtained from the airfoil look-up table as a function of Reynolds number (Re_c) and effective angle of attack, shown in Eq. (8).

$$\mathbf{V}_{\text{inflow}} = \mathbf{V}_{\infty} - \mathbf{\Omega} \times \mathbf{r} + \mathbf{V}_{\text{ind.blade}} + \mathbf{V}_{\text{ind.wake}} \quad \text{Eq. (6)}$$

$$\alpha_{\text{eff}} = \alpha_{\text{inflow}} - \theta_{geo} = \tan^{-1}\left(\frac{\mathbf{V}_{\text{inflow}} \cdot \mathbf{a}_3}{\mathbf{V}_{\text{inflow}} \cdot \mathbf{a}_1}\right) - (\theta_{twist} + \theta_{pitch}) \quad \text{Eq. (7)}$$

$$C_L = f(Re_c, \alpha_{\text{eff}}), \;\; C_D = g(Re_c, \alpha_{\text{eff}}) \quad \text{Eq. (8)}$$

According to the aerodynamic force conventions for the rotor blade of the wind turbine, other aerodynamic performance coefficients, such as thrust (C_T) and torque (C_Q), are evaluated using lift and drag coefficients in conjunction with their reference angles (α_{inflow}), as in Eq. (9) and Eq. (10), respectively. Thrust and torque coefficients are relative to the rotating plane, after which they are integrated along the span of the blade to compute the total aerodynamic performance, including thrust, torque, and power output.

$$C_T = C_L \cos(\alpha_{\text{infow}}) + C_D \sin(\alpha_{\text{infow}}) \quad \text{Eq. (9)}$$

$$C_Q = C_L \sin(\alpha_{\text{infow}}) - C_D \cos(\alpha_{\text{infow}}) \quad \text{Eq. (10)}$$

2.2 Time-accurate vortex particle method

In the current study, the wind turbine wake originating from the rotor blades is represented by the Lagrangian approach, rather than the Eulerian approach. In the case of the Lagrangian approach, just as with vortex particles, and straight and curved vortex filaments, a grid-free Lagrangian formulation not involving an artificial numerical dissipation is used for wake modeling. Hence, it can provide a physically meaningful solution for simulating wake dynamics and also preserve concentrated vorticity fields and wake structure over a long distance. In this study, NVLM is tightly integrated with VPM for modeling the wind turbine wake flow. A nascent rotor wake shed from the trailing edge of a full span of rotor blades is represented as trailed and shed vortex filaments, and they are spilt into vortex particles. These particles mutually interact with each other and are allowed to freely deform and transport downstream as the wake evolves downstream. These properties are especially useful for investigating complex wake evolution and wake interaction phenomena. The vorticity field can be formulated by a sum of vortex particles as follows:

$$\boldsymbol{\omega}(\mathbf{x},t) = \sum_{i=1}^{p} \boldsymbol{\alpha}_i(t)\zeta_\sigma\left(\mathbf{x} - \mathbf{x}_i(t)\right) \quad \text{Eq. (11)}$$

$$\boldsymbol{\alpha}_i(t) = V_i \boldsymbol{\omega}_i(\mathbf{x}_i, t) \quad \text{Eq. (12)}$$

$$\zeta_\sigma(\mathbf{r}) = \frac{1}{\sigma_3}\frac{15}{8\pi}\left[\left(\frac{|\mathbf{r}|}{\sigma}\right)^2 + 1\right]^{-7/2} \quad \text{Eq. (13)}$$

where $\boldsymbol{\omega}(\mathbf{x},t)$ is the vorticity field in the wake, $\boldsymbol{\alpha}_i(t)$ is a strength vector, $\boldsymbol{\omega}_i(\mathbf{x}_i,t)$ is the vorticity vector, $\mathbf{V}_i$ is the volume of i-th vortex particle, $\mathbf{x}$ is the position vector of an arbitrary point in the field, $\mathbf{x}_i$ is the position vector of the i-th vortex particle, and p is the total number of the vortex particles. Eq. (13) indicates that $\zeta_\sigma(\mathbf{r})$ is the three-dimensional high-order algebraic function with a smoothing radius (σ) for representing the vorticity distribution near the vortex particles [31]. This function is needed to avoid the singularity problem. Meanwhile, $\mathbf{r}$ is the position vector between $\mathbf{x}$ and $\mathbf{x}_i$.

$$\frac{d}{dt}\mathbf{x}(t) = \mathbf{V}_{\text{conv}}(\mathbf{x},t) \quad \text{Eq. (14)}$$

$$\mathbf{V}_{\text{conv}}(\mathbf{x},t) = \mathbf{V}_{\infty} + \mathbf{V}_{\text{ind.blade}} + \mathbf{V}_{\text{ind.wake}} \quad \text{Eq. (15)}$$

$$\mathbf{V}_{\text{ind.wake}}(\mathbf{x},t) = \sum_{i=1}^{p} \mathbf{K}_{\sigma}\left(\mathbf{x} - \mathbf{x}_i(t)\right) \times \boldsymbol{\alpha}_i(t) \quad \text{Eq. (16)}$$

$$\mathbf{K}_{\sigma}(\mathbf{r}) = -\left(\frac{q_{\sigma}(\mathbf{r})}{|\mathbf{r}|^3}\right)\mathbf{r} \quad \text{Eq. (17)}$$

$$q_{\sigma}(\mathbf{r}) = \frac{1}{4\pi}\left(\frac{|\mathbf{r}|}{\sigma}\right)^3\left(\left(\frac{|\mathbf{r}|}{\sigma}\right)^2 + \frac{5}{2}\right)\left[\left(\frac{|\mathbf{r}|}{\sigma}\right)^2 + 1\right]^{-5/2} \quad \text{Eq. (18)}$$

The strength of the recently shed vortex particles was already determined at the previous time step by imposing the Kutta condition on the vortex elements placed at the trailing edge. The wake structure, consisting of vortex particles, evolves downstream during the time-marching steps. To update its geometry, the convection velocity of the vortex particle, which is the sum of the free-stream velocity, the self-induced velocity due to the bound vortices, and the wake-induced velocity due to wake vortices have to be evaluated at each time step, as in Eq. (15). The velocity component induced by the vortex particles is calculated using the Biot–Savart law in Eq. (16), where $\mathbf{u}(\mathbf{x},t)$ is the velocity vector at an arbitrary point ($\mathbf{x}$) in the flow field, and $K_{\sigma}(\mathbf{r})$ is the regularized Biot–Savart kernel in Eq. (17). In addition, Eq. (18) indicates that $q_{\sigma}(\mathbf{r})$ is the integration of the three-dimensional high-order algebraic smoothing function.

A time-integration algorithm is required to conduct an unsteady time-accurate simulation. In this study, the second-order Runge–Kutta method is adopted to simulate the wake flow and describe the vorticity fields behind the rotor blades. A further detailed description and validation of NVLM and VPM used in this study are discussed in the references [13, 14, 29].

2.3 Rotor blade modeling

In the present study, two small scale wind turbines, TU Delft and NTNU, are considered. Aside from the differences in the rotor geometry and operating conditions, most of the numerical simulation setup, including the time step, number of revolutions, and number of rotor surface grid points, are identical for simulating the two rotor configurations. For the NVLM simulation, the rotor blades of the small-scale wind turbine are modeled by distributing the quadrilateral vortex ring elements along the chordwise and spanwise directions. The surface grid

resolution of each blade is 35 (chordwise) × 50 (spanwise), with a grid clustering near the inboard and outboard locations. Calculations are conducted for a total twenty revolutions, including one revolution of slowly starting rotation to prevent the wake instability problem, where the rotating speed of the wind turbine blade is gradually increased from zero to the designated speed. The step size for the time marching should be small enough to ensure that the unsteady aerodynamic behavior and complex wake evolution can be captured. A time-step discretization $\Delta\psi = 5°$ is used here.

3. Results and discussion

3.1 TU Delft wind turbine model

3.1.1 Experiment and model description

A notable experiment campaign was carried out in an open jet tunnel at the Delft University of Technology (DUT) to investigate the wind turbine aerodynamics and near wake dynamics of a small-scale wind turbine, as shown in Fig. 3. Vermeer et al. [22, 23] conducted the experiments with a 1.2-m-diameter two-bladed wind turbine model to measure both axial forces acting on the rotor blades and tip vortex trajectories under axial-flow conditions. The rotor thrust forces normal to the rotating plane were recorded by the strain gauges, and the tip vortex trajectories, in terms of the axial and radial positions behind the rotor blade, were captured by the flow visualization technique using a hot-wire probe. A subsequent experiment was performed by Haans et al. [24, 25], which was a follow up of the first experiment with similar wind turbine configuration and flow conditions. In the second experiment, the hub shape was changed from a sharp-edged cubic sphere to a half-sphere, and the near-wake geometry was captured by a smoke visualization technique, rather than a hot wire probe. Moreover, the yawed-flow conditions, as well as the axial-flow conditions, were considered in the second experiment. A detailed description with regard to the wind turbine model is listed in Table 1, and the rotor planform geometry, in terms of chord length and twist angle, is illustrated in Fig. 4. In the present study, only wind turbine blade without hub and tower configuration is considered. During the wind tunnel experiment, the TU Delft wind turbine model was subjected to various operating conditions including tip speed ratio, tip pitch angle, and yaw angle, as listed in Table 2. The wind speed remained constant, while the rotor speed was changed to adjust the tip speed ratio.

The TU Delft experiment provided extensive data on the integrated thrust force and tip vortex trajectories of the small-scale wind turbine under axial- and yawed-flow conditions, where operating conditions correspond to the low-Reynolds-number flow, as shown in Table 2. Therefore, calculations for the TU Delft rotor configuration

can be used to validate the predictive capability of NVLM by comparing the aerodynamic loads and near-wake structures against the measurements [24, 25]. In addition, the effects of nonlinear aerodynamic behavior associated with low-Reynolds-number flow on wind-turbine aerodynamics and wake dynamics are clearly observed.

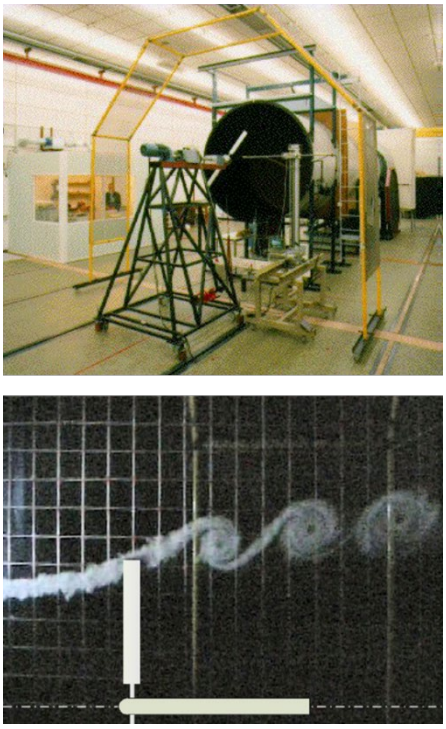

Fig. 3. Open jet wind tunnel facility in DUT and smoke visualization technique [24, 25]

Table 1. Description of TU Delft wind turbine

Parameter	Value
Rotor configuration	Upwind
Number of blades, N [-]	2
Rotor radius, R [m]	0.6
Hub radius, R_h [m]	0.18
Tip chord length, c_{tip} [m]	0.08
Hub tilt angle, γ_{tilt} [deg.]	0
Blade coning angle, β_{cone} [deg.]	0
Blade planform	Rectangular-twisted blade
Blade sectional profile	NACA 0012 airfoil

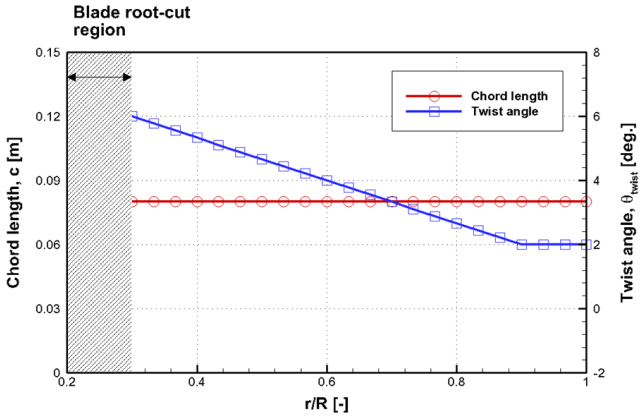

Fig. 4. Planform geometry of TU Delft rotor blade

Table 2. Axial and yawed flow conditions for TU Delft rotor simulation

Parameter	Value
Reynolds number, Re_c [-]	40,000~310,000
Wind speed, V_∞ [m/s]	5.5
Tip speed ratio, λ [-]	6, 8, 10
Tip pitch angle, θ_{tip} [deg.]	0, 2, 4
Yaw angle, β [deg.]	0, ±15, ±30, ±45

3.1.2 Axial flow conditions

To clearly figure out the differences between the VLM and NVLM results, the predicted thrust forces acting on the TU Delft rotor blade exposed to the axial-flow conditions are separately compared with the measurements, as shown in Figs. 5 and 6, respectively. The effects of the tip pitch angle on the aerodynamic loads are well observed from both numerical simulations. In the wind turbine aerodynamics, if the tip pitch angle increases under constant tip speed ratio conditions, the local angle of attack decreases, leading to a decrease in the thrust force. Although both numerical methods are able to derive similar results qualitatively, a noticeable difference is observed quantitatively. Comparison results show that the thrust forces calculated from the NVLM simulation are well-matched with the experimental data, whereas VLM results tend to significantly under-estimate the aerodynamic loads. It is found that the NVLM simulation yields much more accurate results, with an average error of 2.43%. However, the average error of VLM prediction is over 17.84%. In addition, Fig. 5 shows that the numerical error of VLM results increases as the tip speed ratio or tip pitch angle increases. An overall under-prediction in the thrust force is thought to be due to the limitations in the prediction capability of VLM associated

with the intrinsic assumption of linear potential theory. This suggests that numerical remedies, such as a sectional airfoil look-up table and vortex strength correction, used in NVLM to consider nonlinear aerodynamic characteristics, are needed to correctly predict the aerodynamic performance of the scaled-down wind turbine.

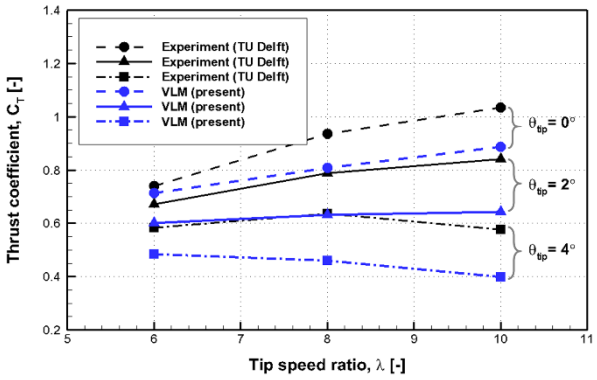

Fig. 5. Thrust coefficient comparison between the measurements [25] and VLM results at the axial flow conditions

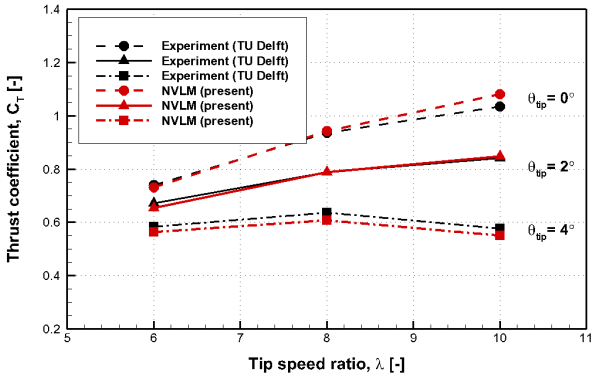

Fig. 6. Thrust coefficient comparison between the measurements [25] and NVLM results at the axial flow conditions

The wind turbine captures the kinetic energy of the incoming wind to produce electrical energy; then, the air passing through the wind turbine slowly moves as a consequence of losing momentum, and the wake generated from the rotor blades expands in the radial direction. For the axial-flow condition, the wind turbine wake evolves in the form of helical geometry and moves downstream. The wake vortices induce the velocity components on the rotor blade, resulting in the variation in angle of attack at the blade sections. Hence, the understanding and accurate prediction of the wind turbine wake are important because its structure is a critical factor in determining

wind turbine performance. As mentioned before, in the present study, the wind turbine wake is modeled by Lagrangian-based vortex particles. The wind turbine wake consisting of vortex particles and tip vortices measured by smoke visualization (denoted by black circle symbol) are shown in Fig. 7. In addition, to assess the effects of low-Reynolds-number flow on the wake structure, the tip vortex trajectories with respect to wake age are also computed by using VLM (denoted by blue square symbol). The helical geometry of the wind turbine wake is easily noticeable in the NVLM simulation, and the wake can be preserved up to the far-field without undesirable dissipation error, even beyond the two rotor diameter downstream. Fig. 7 presents that the NVLM simulation well captures the development of the helical wake structures, and the near-wake geometries in terms of axial and radial positions with respect to time are in good agreement with the measured data, although the radial positions are slightly under-predicted. It turns out that NVLM is shown to be capable of accurately modeling the wake structure of the small-scale wind turbine as well as the aerodynamic loads. However, VLM simulation tends to over-predict the axial position of the helical wake structure, even though the predictions in the radial positions obtained by the VLM and NVLM appear to be similar. This observation is consistent with our earlier findings about the predicting thrust forces. As discussed above, VLM has inherent shortcoming in considering nonlinear aerodynamic characteristics; hence, this limitation inevitably incurs an inaccurate prediction of the rotor performance, particularly the small-scaled wind turbine operating in low Reynolds number flow. The overall thrust coefficients obtained by the VLM simulation are lower than the experimental data, as shown in Fig. 5. The underestimation of the thrust force has a direct bearing on the over-prediction of the radial position of the helical wake structure because the smaller the thrust force acting on the rotor blade is, the farther the wake can be propagated from the wind turbine as a result of decreasing axial momentum reduction. A close relationship between the thrust force and wake propagation can also be observed in Fig. 7. Under the same tip speed ratio conditions, if the tip pitch angle increases from (a) to (c) in Fig. 7, the thrust force decreases owing to the reduction in the local angle of attack. This indicates that the momentum reduction in the axial direction decreases, leading to a decrease in the wake expansion angle and an increase in the helical pitch of the wake geometry. Consequentially, the wind turbine wake can be propagated further downstream at a tip pitch angle of 4°, compared to the tip pitch angle of 0°.

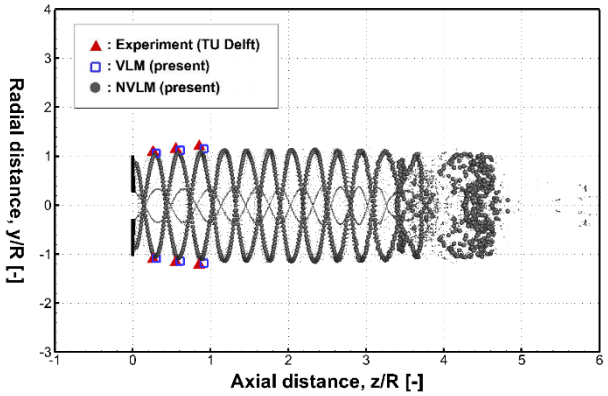

(a) tip pitch angle of 0°

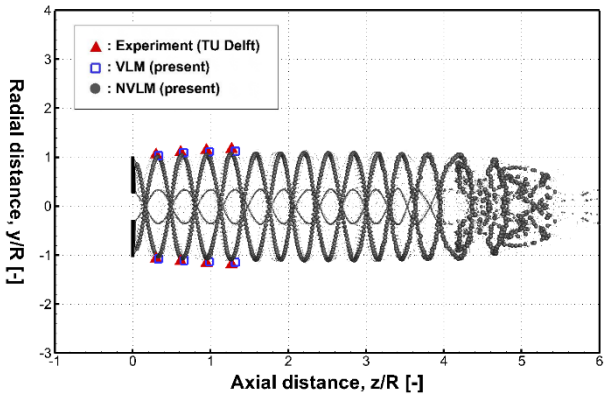

(b) tip pitch angle of 2°

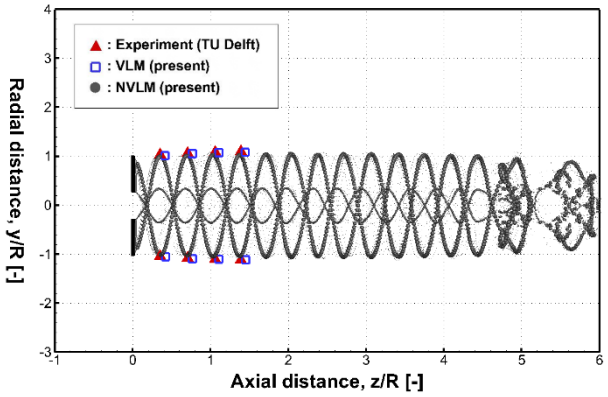

(c) tip pitch angle of 4°

Fig. 7. Comparison of the measured and predicted tip vortex trajectories for the axial flow conditions

3.1.3 Yawed flow conditions

The yawing angle has a direct impact on the aerodynamic performance and development of the wind turbine wake. When the wind turbine is exposed to yawed-flow conditions, the wind turbine wake behind the rotor disc evolves with a deflection angle. The skewed wake structure causes an asymmetric distribution of wake-induced velocity at the rotating plane; this causes the local angle of attack at the blade sections and resulting forces to periodically change, owing to advancing and retreating effects. Then, the flow physics around the rotor blades become highly unsteady and complicated. Moreover, the wake behavior downstream becomes unstable because a strong wake interaction between the tip and hub wake vortices occurs owing to the skewed wake geometry. It is important to consider the complex wake characteristics for accurately analyzing the yaw aerodynamics. Predicting unsteady aerodynamic loads and capturing the wake geometry of the wind turbine under the yawed flow conditions are still one of the main challenging problems in the wind turbine field.

Numerical simulation of the TU Delft rotor with various tip pitch and yaw angles at a constant tip speed ratio ($\lambda = 8$) was carried out. Time-averaged thrust forces are computed by VLM and NVLM simulations, and they are compared with experimental data, as shown in Figs. 8 and 9, respectively. The predicted time-averaged results help in understanding the fundamental yaw aerodynamics of the wind turbine. As the yaw angle increases, the velocity normal to the rotating plane decreases, whereas the velocity tangential to the rotating plane increases where the radial flow becomes dominant over the rotor blade. A reduction in the magnitude of the velocity component aligned normal to the rotating plane results in a decrease in the angle of attack at the blade section. Eventually, the time-averaged thrust force gradually decreases with increasing yaw angle from 0° to 45°. It can be also observed that the thrust force decreases with an increase in tip pitch angle, as discussed in the axial flow condition case. The comparison between Figs. 8 and 9 indicates that the NVLM results show excellent agreement with the measurements, even for highly yawed-flow conditions, whereas VLM significantly under-predicts the aerodynamic loads. It is found that the NVLM simulation yields much more accurate results, with an average error of 3.48%. However, the average error of VLM prediction is over 20.12%, which implies that the highly unsteady flow phenomena caused by the yawed inflow and nonlinear aerodynamic characteristics associated with low-Reynolds-number flow are well captured by the present method. This helps to accurately predict the performance of the small-scale wind turbine under yawed-flow conditions.

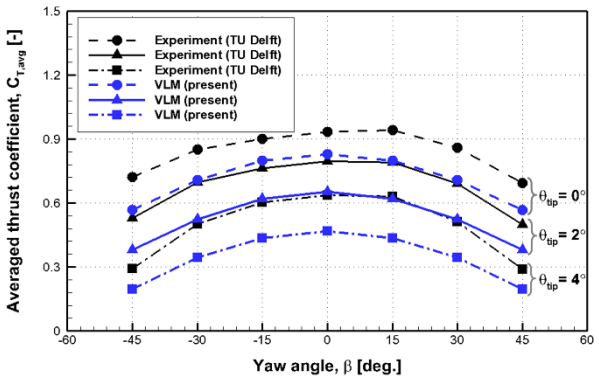

Fig. 8. Thrust coefficient comparison between the measurements [25] and VLM results at the yawed flow conditions

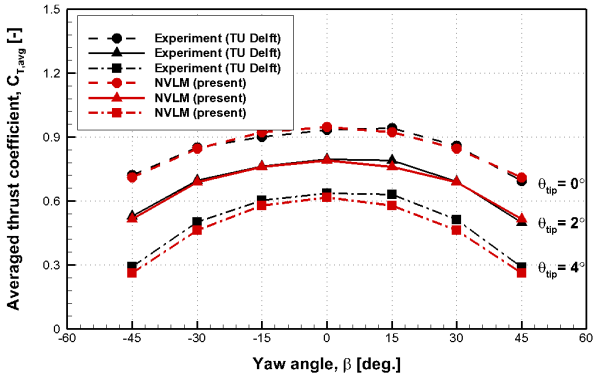

Fig. 9. Thrust coefficient comparison between the measurements [25] and NVLM results at the yawed flow conditions

Fig. 10 clearly presents the skewed wake geometry of the TU Delft wind turbine under yawed-flow conditions. Further evidence of the improvement associated with the consideration of low-Reynolds-number flow effects can be observed in the prediction of the wake geometry. Skewed wake geometries depending on the tip pitch angle are predicted from VLM and NVLM simulations, and they are compared against the measurements. The predictions in terms of the axial and radial positions of the near-field wake structure appear to be similar; however, the obtained results from the NVLM simulation are in better agreement with the measured data. NVLM results show that the tip vortex trajectories of the near-wake on the upwind side are well-matched with the measurements, while those on the downwind side are slightly overestimated.

As shown in Figs. 7 and 10, the present method used in this study provides a meaningful wake solution for both the axial- and yawed-flow conditions. The visualized wake structures of the wind turbine are presented here

to provide significant insight into the wake dynamics. The wind turbine wake is developed in the form of the helical geometry for the axial-flow condition, whereas the tip vortices expand unequally, resulting in a strong expansion downwind side and a weak expansion upwind side for the yawed-flow condition. The trailing tip vortices are located closer to the downwind side of the rotor blade than the upwind side because of the skewed wake geometry. The wake vortices shed from the upwind side eventually become unstable and begin to interact with the wake vortices placed on the downwind side. The wake-to-wake interaction effect is manifested as the wake evolves downstream. Finally, the skewed wake structures completely break down and merge to form a mixing region at the far-field. This is called the tip vortex breakdown phenomenon. Consequentially, it is found that the deflected wake geometry makes the trailing and shed wake vortices interact strongly with each other, leading to a much faster destruction of the wake structure and a transition into the turbulent wake state, compared with under the axial-flow conditions.

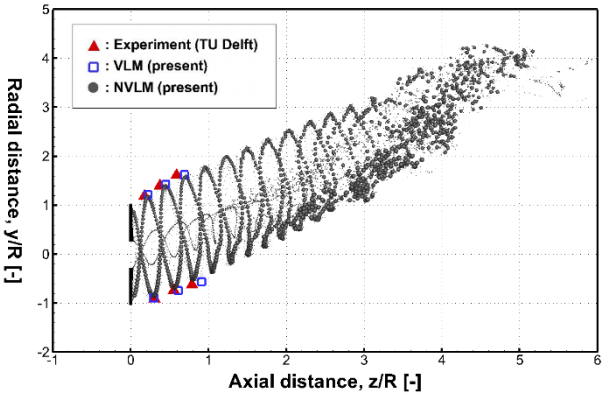

(a) tip pitch angle of 0°

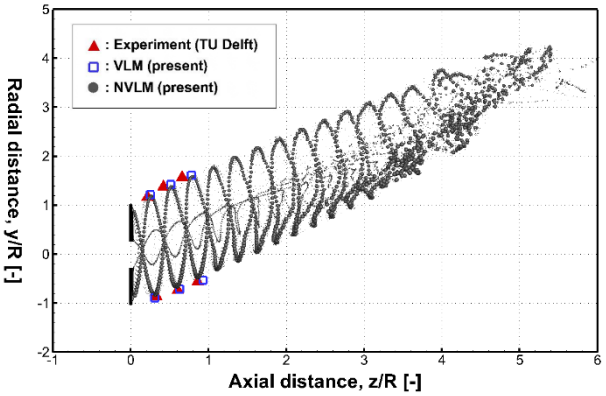

(b) tip pitch angle of 2°

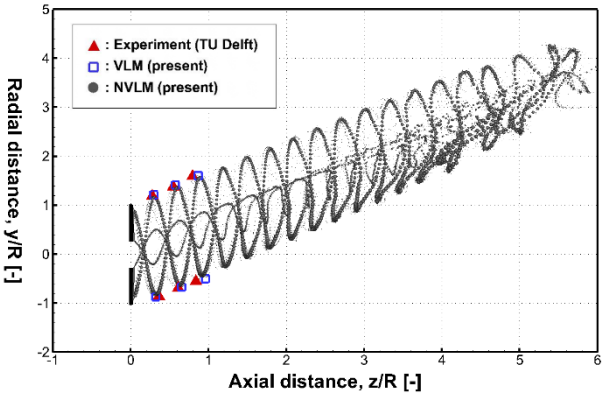

(c) tip pitch angle of 4°

Fig. 10. Comparison of the measured and predicted tip vortex trajectories for the yawed flow conditions

3.2 NTNU wind turbine model

3.2.1 Experiment and model description

Another set of small-scale wind turbine experiment was conducted by the joint Norwegian research programs on wind turbine technology, denoted Nowitech and Norcowe. After the measurements, they organized the first blind test workshop using an isolated wind turbine configuration in 2011, as shown in Fig. 11. In 2012, a more complicated second blind test workshop as a follow up of the first test campaign, using two similar turbines operating in line, was carried out. The main aim of this experiment was to obtain reliable and useful data for validating the current prediction models of wind-turbine performance, such as BEM, actuator disk or actuator line theories, vortex methods, and CFD methods. The measurements were taken on the three-bladed wind turbine model in the large-scale closed-loop wind tunnel facility of Norwegian University of Science and Technology (NTNU), where the rectangular test section of the wind tunnel is 2.71 m wide, 1.81 m high, and 11.14 m long. This experiment provided a comprehensive high-quality database, including the tables of power and thrust coefficients as a function of tip speed ratio. The radius of the rotor blade is 0.447 m, and the hub height is 0.817 m above the floor level. The rotor blade is composed of the NREL S826 airfoil along the entire rotor span, except for the last circular section as listed in Table 3, and the planform geometry of the rotor blade as a function of radial position is depicted in Fig. 12. In the present study, only wind turbine blade without hub and tower configuration is considered. The experimental study also provided the normalized mean velocity defect and turbulent kinetic energy along the horizontal and vertical traverses at the positions of 1D, 3D, and 5D downstream. Here, D is the

rotor diameter. The measurements can help to achieve a better understanding of the wake flow field of the wind turbine. However, validating the wake flow is out of the scope of this paper, and it will be discussed in future studies.

The wind turbine model is subjected to various tip speed ratios, from 1 to 12, while the wind speed remains constant. The operating conditions for the wind turbine experiment are listed in Table 4. The NTNU wind turbine model operates under the low-Reynolds-number flow condition, as the blade radius is 0.447 m. The Reynolds number, based on the tip chord length (Re_c) at the designated tip speed ratio, is approximately 10^5. Hence, it is important to take into account the low-Reynolds-number effects on the rotor performance.

Fig. 11. Closed-loop wind tunnel facility in NTNU and scaled-down wind turbine model [26]

Table 3. Description of NTNU wind turbine model

Parameter	Value
Rotor configuration	Upwind
Number of blades, N [-]	3
Rotor radius, R [m]	0.447
Hub radius, R_h [m]	0.045
Tip chord length, c_{tip} [m]	0.0258
Hub tilt angle, γ_{tilt} [deg.]	0
Blade coning angle, β_{cone} [deg.]	0
Blade planform	Tapered-twisted blade
Blade sectional profiles	S826 airfoil

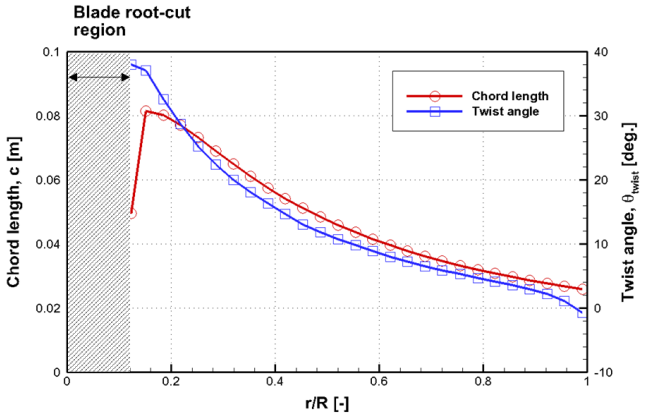

Fig. 12. Planform geometry of NTNU rotor blade

Table 4. Axial flow conditions for NTNU rotor simulation

Parameter	Value
Reynolds number, Re_c [-]	10,000~300,000
Wind speed, V_∞ [m/s]	10
Tip speed ratio, λ [-]	1~12
Tip pitch angle, θ_{tip} [deg.]	0
Yaw angle, β [deg.]	0

3.2.2 Aerodynamic loads

To investigate the effect of low-Reynolds-number flow on the aerodynamic performance of the small-scale wind turbine, NTNU rotor blades are tested under axial flow conditions. Both the thrust and power coefficients of the NTNU wind turbine model are predicted and compared against the measurements, as shown in Figs. 13 and 14, respectively. Fig. 13 presents the variation of the thrust coefficients with increasing tip speed ratio under a constant incoming wind speed, namely, an increasing rotation rate. Whereas the VLM results show a significant over-prediction in the thrust coefficients for a wide range of operating conditions, the NVLM simulation yields more accurate results. The improvement associated with the considering low-Reynolds-number effects is easily noticeable, particularly under low tip speed ratio conditions where the rotor blades could experience flow separation owing to the high angle of attack and dynamic stall behavior. Similar results are observed for predicting the power coefficients of the NTNU wind turbine model. Fig. 14 shows that the optimal tip speed ratio condition of the NTNU wind turbine model, which can generate the maximum power output, is well predicted from both the NVLM and VLM simulations. NVLM predictions show an overall agreement with the measured data for a

range of tip speed ratios. It can be seen that there is a significant improvement in predicting the power coefficients of the small-scale wind turbine. As a result, the overall performance of the NTNU wind turbine model, including the thrust force and power output, can be well predicted from the NVLM simulation. However, there is a discernible difference between the experiments and the VLM results. Prediction error becomes highly significant when the rotor blade operates at a higher and a lower tip speed ratio. Numerical errors occur, which may be due to the neglect of nonlinear aerodynamic behavior mainly associated with flow separation at the low tip speed ratio and aerodynamic losses from the airfoil drag at high tip speed ratio.

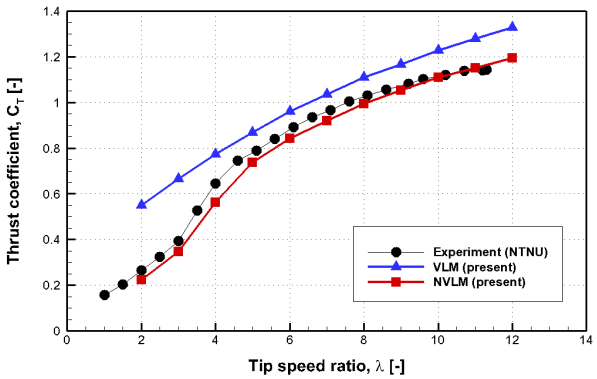

Fig. 13. Thrust coefficient comparison between the measurements [26] and predicted results

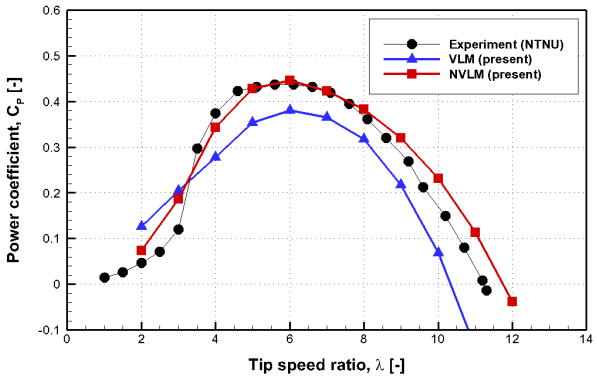

Fig. 14. Power coefficient comparison between the measurements [26] and predicted results

4. Conclusion

This study has brought up a numerical issue related to the limitations of the prediction capability of VLM models that appears for small-scale wind turbines operating in low-Reynolds-number flow. VLM tends to suffer from numerical error under these conditions because it inherently cannot handle the nonlinear aerodynamic

characteristics caused by the viscous effects and laminar boundary-layer separation. In the present study, an NVLM model, incorporating a sectional airfoil look-up table and vortex strength correction, was adopted to predict the aerodynamic performance of the small-scale wind turbine. The results obtained from the VLM and NVLM simulations were compared against the measurements to validate the predictive capability of the numerical models. It was shown that NVLM appears to be an effective and useful method for resolving the shortcomings of the VLM.

In this study, two small-scale wind turbines, TU Delft and NTNU, were considered. Numerical simulation of the TU Delft wind turbine was conducted under both axial- and yawed-flow conditions to investigate the effects of low-Reynolds-number flow on the near wake structure of the wind turbine as well as the aerodynamic performance. The thrust forces and tip vortex trajectories of the TU Delft wind turbine model were predicted and compared with measurements. The variation of thrust forces with respect to the tip speed ratio, tip pitch angle, and yaw angle were captured well by the present method, whereas VLM yielded significantly under-predicted results. NVLM results also showed that the helical and skewed wake geometries as a function of axial and radial positions are in better agreement with the measured data. It was concluded that the effects of low-Reynolds-number flow should be considered to numerically analyze the wake dynamics as well as rotor aerodynamics of the small-scale wind turbine. In addition, the wake dynamics of the wind turbine were analyzed in detail. This information can help to achieve a better understanding of complex wake phenomena, such as wake-to-wake interaction, tip vortex breakdown, and wake deflection. The thrust and power coefficients of the NTNU wind turbine model under axial-flow conditions were computed. A comparison between the measured data and NVLM predictions showed overall agreement for a range of tip speed ratios, particularly for low tip speed ratios for which flow separation and dynamic stall behavior occur due to the high angle of attack. However, VLM failed to capture the aerodynamic performance of small-scale wind turbine models. Therefore, for the case of such small-scale wind turbines in which the effects of viscous and low-Reynolds-number flow are dominant, NVLM appears to be a suitable and computationally efficient model.

Declaration of interest

There is no conflict of interest

Acknowledgments

This work was supported by the Korea Institute of Energy Technology Evaluation and Planning (KETEP) and the Ministry of Trade, Industry & Energy (MOTIE) of the Republic of Korea (No. 20168520021200).

References

[1] M.M. Hand, D.A. Simms, L.J. Fingersh, D.W. Jager, J.R. Cotrell, S. Schreck, S.M. Larwood, "Unsteady Aerodynamics Experiment Phase VI: Wind Tunnel Test Configurations and Available Data Campaigns," Technical Report, NREL/TP-500-29955, 2001.

[2] J.G. Schepers, K. Boorsma, T. Cho, S. Gomez-Iradi, P. Schaffarczyk, A. Jeromin, W.Z. Shen, T. Lutz, K. Meister, B. Stoevesandt, S. Schreck, D. Micallef, R. Pereira, T. Sant, H.A. Madsen, N. Sørensen, "Final Report of IEA Task 29, Mexnext (Phase 1): Analysis of Mexico Wind Tunnel Measurements," Technical Report, ECNE12-004, Energy Research Center of the Netherlands, 2012.

[3] J.G. Schepers, K. Boorsma, S. Gomez-Iradi, P. Schaffarczyk, H.A. Madsen, N.N. Sørensen, W.Z. Shen, T. Lutz, C. Schulz, I. Herraez, S. Schreck, "Final Report of IEA Wind Task 29: Mexnext (Phase 2)," Technical Report, ECN-Ed14-060, Energy Research Center of the Netherlands, 2014.

[4] K.W. Ryu, S.H. Kang, Y.H. Seo, W.R. Lee, "Prediction of aerodynamic loads for NREL Phase VI wind turbine blade in yawed condition," *Int. J. Aeronaut. Space Sci.* 17 (2) (2016) 157-166.

[5] B. Plaza, R. Bardera, S. Visiedo, "Comparison of BEM and CFD results for MEXICO rotor aerodynamics," *Journal of Wind Engineering and Industrial Aerodynamics* 14 (2015) 115-122.

[6] W.Z. Shen, W.J. Zhu, J.N. Sørensen, "Actuator line/Navier–Stokes computations for the MEXICO rotor: comparison with detailed measurements," *Wind Energy*, 15 (5) (2012) 811-825.

[7] S. Samast, W.Z. Shen, W.J. Zhu, R.F. Mikkelsen, S.P. Breton, S. Ivanell, "Validation of the actuator line and disc techniques using the New Mexico measurements," *J. Phys. Conf.* 723 (2016), 032026.

[8] S.P. Breton, W.Z. Shen, S. Ivanell, "Validation of the actuator disc and actuator line techniques for yawed rotor flows using the New MEXICO experimental data," *J. Phys. Conf.* 854 (2017), 012005.

[9] T. Sant, G. van Kuik, G.J.W. van Bussel, "Estimating the Angle of Attack from Blade Pressure Measurements on the NREL Phase VI Rotor Using a Free Wake Vortex Model: Axial Conditions," *Wind Energy*, 9 (6) (2006) 549-577.

[10] T. Sant, G. van Kuik, G.J.W. van Bussel, "Estimating the Angle of Attack from Blade Pressure Measurements on the National Renewable Energy Laboratory Phase VI Rotor Using a Free Wake Vortex Model: Yawed Conditions," *Wind Energy*, 12 (1) (2009) 1-32.

[11] F. Blondel, B. Boisard, M. Milekovic, G. Ferrer, C. Lienard, D. Teixeira, "Validation and comparison of aerodynamic modelling approaches for wind turbines," *J. Phys. Conf.* 723 (2016), 022029.

[12] H. Abedi, L. Davidson, S. Voutsinas, "Enhancement of free vortex filament method for aerodynamic loads on rotor blades," *J. Sol. Energy Eng.* 139 (3) (2017), 031007.

[13] H. Lee, D.J. Lee, "Numerical investigation of the aerodynamics and wake structures of horizontal axis wind turbines by using nonlinear vortex lattice method," *Renew. Energy* 132 (2019) 1121-1133.

[14] H. Lee, D.J. Lee, "Wake impact on aerodynamic characteristics of horizontal axis wind turbine under yawed flow conditions," *Renew. Energy* 136 (2019) 383-392.

[15] E.P.N. Duque, M.D. Burklund, W. Johnson, "Navier-Stokes and comprehensive analysis performance predictions of the NREL Phase VI experiment," *J. Sol. Energy Eng.* 125 (4) (2003) 457-467.

[16] C. Tongchitpakdee, S. Benjanirat, L.N. Sankar, "Numerical simulation of the aerodynamics of horizontal Axis wind turbines under yawed flow conditions," *J. Sol. Energy Eng.* 127 (4) (2005) 464-474.

[17] A. Bechmann, N.N. Sørensen, F. Zahle, "CFD simulations of the MEXICO rotor," *Wind Energy* 14 (5) (2011) 677-689.

[18] D.O. Yu, J.Y. You, O.J. Kwon, "Numerical investigation of unsteady aerodynamics of a horizontal-axis wind turbine under yawed flow conditions," *Wind Energy* 16 (2013) 711-727.

[19] M. Carrión, R. Steijl, M. Woodgate, G. Barakos, X. Munduate, S. Gomez-Iradi, "Computational fluid dynamics analysis of the wake behind the MEXICO rotor in axial flow conditions," *Wind Energy* 18 (6) (2015) 1023-1045.

[20] N.N. Sørensen, F. Zahle, K. Boorsma, G. Schepers, "CFD computations of the second round of Mexico rotor measurements," *J. Phys. Conf.* 753 (2016), 022054.

[21] K. Lee, S. Roy, Z. Huque, R. Kommalapati, S.E. Han, "Effect on Torque and Thrust of the Pointed Tip Shape of a Wind Turbine Blade," *Energies*, 10 (1) (2017) 79.

[22] L.J. Vermeer, "A Review of Wind Turbine Wake Research at TU Delft. 20th 2001 ASME Wind Energy Symposium," 39th Aerospace Sciences Meeting and Exhibit, AIAA-2001-0030, Reno, NV, U.S.A., January 11-14, 2001.

[23] L.J. Vermeer, J.N. Sørensen, A. Crespo, "Wind Turbine Wake Aerodynamics," *Progress in Aerospace Sciences* 2003, 39, 467-510.

[24] W. Haans, T. Sant, G. van Kuit, G. van Bussel, "Measurement and Modelling of Tip Vortex Paths in the Wake of a HAWT under Yawed Flow Conditions," 43rd AIAA Aerospace Sciences Meeting and Exhibit, AIAA 2005-590, Reno, NV, U.S.A., January 10-13, 2005.

[25] W. Haans, T. Sant, G. van Kuik, G. van Bussel, "Measurement of Tip Vortex Paths in the Wake of a HAWT Under Yawed Flow Conditions," *J. Sol. Energy Eng.* 127 (4) (2005) 456-463.

[26] P.Å. Krogstad, P.E. Eriksen, ""Blind test" calculations of the performance and wake development for a model wind turbine," *Renew. Energy*, 50 (2013) 325-333.

[27] F. Pierella, P.Å. Krogstad, Lars Sætran, "Blind Test 2 calculations for two in-line model wind turbines where the downstream turbine operates at various rotational speeds," *Renew. Energy*, 70 (2014) 62-77.

[28] W. Du, Y. Zhao, M. Wang, Y. He, R. Jiang, "Design and Analysis of a Model Wind Turbine Blade for Wave Basin Test of Floating Wind Turbines," 2013 International Offshore and Polar Engineering, Anchorage, Alaska, U.S.A, June 30-July 5, 2013.

[29] H. Lee, D.J. Lee, "Effects of platform motions on aerodynamic performance and unsteady wake evolution of a floating offshore wind turbine," *Renew. Energy*, 2019, 143 (2019) 9-23.

[30] J. Katz, A. Plotkin, "Low-Speed Aerodynamics, 2nd ed.," Cambridge Univ. Press, Cambridge, England, U.K., 2001.

[31] G.S. Winckelmans, A. Leonard, "Contributions to Vortex Particle Methods for the Computation of Three-Dimensional Incompressible Unsteady Flows," *J. Comput. Phys.* 109 (1993) 247-273.